


Elevated transition temperature in Ge doped VO₂ thin films

Cite as: J. Appl. Phys. **122**, 045304 (2017); <https://doi.org/10.1063/1.4995965>

Submitted: 05 April 2017 . Accepted: 13 July 2017 . Published Online: 27 July 2017

Anna Krammer, Arnaud Magrez, Wolfgang A. Vitale, Piotr Mocny, Patrick Jeanneret , Edouard Guibert, Harry J. Whitlow, Adrian M. Ionescu, and Andreas Schüler



View Online



Export Citation



CrossMark

ARTICLES YOU MAY BE INTERESTED IN

[Roles of strain and domain boundaries on the phase transition stability of VO₂ thin films](#)

Applied Physics Letters **111**, 153102 (2017); <https://doi.org/10.1063/1.4991882>

[Optimizing thermochromic VO₂ by co-doping with W and Sr for smart window applications](#)

Applied Physics Letters **110**, 141907 (2017); <https://doi.org/10.1063/1.4979700>

[A metal-insulator transition study of VO₂ thin films grown on sapphire substrates](#)

Journal of Applied Physics **122**, 235102 (2017); <https://doi.org/10.1063/1.4997437>



Lock-in Amplifiers

Zurich Instruments

Watch the Video

Elevated transition temperature in Ge doped VO₂ thin films

Anna Krammer,^{1,a)} Arnaud Magrez,² Wolfgang A. Vitale,³ Piotr Mocny,⁴ Patrick Jeanneret,⁵ Edouard Guibert,⁵ Harry J. Whitlow,^{5,b)} Adrian M. Ionescu,³ and Andreas Schüler¹

¹Solar Energy and Building Physics Laboratory (LESO-PB), EPFL, Lausanne CH-1015, Switzerland

²Institute of Condensed Matter Physics (ICMP), EPFL, Lausanne CH-1015, Switzerland

³Nanoelectronic Devices Laboratory (NanoLab), EPFL, Lausanne CH-1015, Switzerland

⁴Polymers Laboratory (LP), EPFL, Lausanne CH-1015, Switzerland

⁵Surface Engineering Group (Ionlab-Arc), University of Applied Sciences (HES-SO), La Chaux-de-Fonds CH-2300, Switzerland

(Received 5 April 2017; accepted 13 July 2017; published online 27 July 2017)

Thermochromic Ge_xV_{1-x}O_{2+y} thin films have been deposited on Si (100) substrates by means of reactive magnetron sputtering. The films were then characterized by Rutherford backscattering spectrometry (RBS), four-point probe electrical resistivity measurements, X-ray diffraction, and atomic force microscopy. From the temperature dependent resistivity measurements, the effect of Ge doping on the semiconductor-to-metal phase transition in vanadium oxide thin films was investigated. The transition temperature was shown to increase significantly upon Ge doping (~95 °C), while the hysteresis width and resistivity contrast gradually decreased. The precise Ge concentration and the film thickness have been determined by RBS. The crystallinity of phase-pure VO₂ monoclinic films was confirmed by XRD. These findings make the use of vanadium dioxide thin films in solar and electronic device applications—where higher critical temperatures than 68 °C of pristine VO₂ are needed—a viable and promising solution. *Published by AIP Publishing.*

[<http://dx.doi.org/10.1063/1.4995965>]

I. INTRODUCTION

Thermochromic VO₂ is an emblematic strongly correlated material which undergoes a fully reversible first order semiconductor-to-metal transition (SMT), from the monoclinic (P2₁/c) to tetragonal (P4₂/mmm) crystal structure, at 68 °C.^{1–3} The ultrafast, sub-picosecond transition^{4,5} is marked by abrupt changes in electrical (~4 orders of magnitude resistivity drop) and optical properties (dielectric constants vary strongly, particularly in the IR range).^{6–8}

Due to the ultrafast SMT and its relative closeness to room temperature, vanadium dioxide has raised overwhelming interest in both fundamental research and a variety of applications. Most recently,⁹ an order-of-magnitude breakdown of the Wiedemann-Franz law has been reported in metallic VO₂ in the vicinity of the semiconductor-to-metal transition. Moreover, VO₂ became a prominent candidate for ultrafast optical and electrical switches,^{10,11} tunable capacitors,¹² microbolometers,¹³ smart windows,^{14,15} smart radiators in solar thermal¹⁶ or space¹⁷ applications, etc. For practical applications, various transition temperatures are desired and, through doping, the phase transition temperature can be tailored to fit a wide range of requirements. The origin of the SMT in phase-pure VO₂ and the mechanisms through which dopant elements inflict their effect on it is still an open subject despite the extensive research and decade-long debates on the topic.^{4,18–21} Nonetheless, it is generally believed that donor-like dopants with large ionic radii (W⁶⁺, Mo⁶⁺, and Nb⁵⁺) decrease the transition temperature T_{SMT}, while acceptor-like elements of low oxidation state and smaller ionic radii (Al³⁺,

Cr³⁺, Fe³⁺) increase T_{SMT}.³ Tungsten has been considered the most efficient among dopants, enabling a reduction in T_{SMT}, with a nearly linear rate of 49–55 °C/at. % W dopant.²² However, shifting the SMT temperature in the other direction is less efficient and less studied. Introduction of smart thermochromic VO₂ based solar thermal collectors¹⁶ and recent developments at the microelectronic device level^{11,12} emphasize the importance of a reliable, inexpensive, and efficient doping that enables a precise control over a wide range of elevated T_{SMT} in vanadium dioxide thin films. Studies on dopants shown to increase the transition temperature were mainly published for single crystal or powder VO₂.^{23–25} When going to thin films, the effect of such doping elements is not evident and proved to be controversial. In contrast to expectations, Al³⁺ doping decreased the transition temperature and induced progressive amorphization of the VO₂ films.^{22,26,27} Fe³⁺ was also reported to decrease the transition temperature in thin films,²⁸ while Cr³⁺ has been shown to increase it to not more than 70 °C.²⁹

In a 1968 patent, Futaki *et al.*³⁰ reported elevated transition temperatures in Ge doped VO₂ crystals. From thereon, Ge was much referred to as a dopant which increases the SMT temperature and it was widely assumed that this effect would be applicable to thin films too. However, to the best of our knowledge, the latter was never looked into. In the present letter, we aim to study the effect of Ge doping on vanadium dioxide thin films and we report the effective increase in the critical transition temperature of such VO₂ films.

II. EXPERIMENTAL DETAILS

A. Film growth

Vanadium dioxide based thin films, with different Ge contents, were deposited by reactive magnetron sputtering in

^{a)}Electronic mail: anna.krammer@epfl.ch.

^{b)}Present address: Louisiana Accelerator Center and Department of Physics, University of Louisiana at Lafayette, Lafayette, LA 70506 USA.

high-vacuum conditions. The base pressure of the chamber was kept below 5×10^{-8} mbar. 480–580 nm thick films were co-sputtered from V (99.95%) and Ge (99.999%) targets on $\langle 100 \rangle$ Si substrates. The power applied on the Ge source was varied, thus changing the composition of different samples. All the other deposition parameters were kept constant.

The oxygen pressure during deposition was kept constant by a Proportional Integral Derivative (PID) feedback control. It regulated the oxygen flow based on the pressure readings of a Zirox XS22 lambda-probe oxygen sensor. The process pressure was $7.73 \pm 0.2 \times 10^{-3}$ mbar, and the oxygen partial pressure was $4.14 \pm 0.2 \times 10^{-4}$ mbar. The temperature was kept constant at 640 °C. The detailed sample preparation has been previously reported elsewhere.^{22,31}

B. Film characterization

Precise Ge quantification in the $\text{Ge}_x\text{V}_{(1-x)}\text{O}_{2+y}$ thin films and determination of film thicknesses were achieved by Rutherford Backscattering Spectrometry (RBS). The data were collected using a 1.7 MV tandemron accelerator with a 2 MeV He^{2+} ion beam. The incident angle of the ion beam was 0°, normal to the sample surface, while backscattered particles were detected at a scattering angle of 150°. Data analysis was done using the Ion Beam Analysis DataFurnace code.³²

The thermochromic properties of the films were studied from room temperature up to 120 °C by determining their temperature dependent electrical resistivity. This was done by standard four-point probe measurements using a semiconductor parameter analyzer (HP 4156C) and a control on the sample temperature up to 120 °C.

The crystallinity and phase composition of the deposited films were determined at room temperature by grazing incidence X-ray diffraction (GIXRD, Empyrean system equipped with a PIXcel-1D detector, monochromatic Cu K α radiation, a grazing incidence GI angle of 4°). The surface topography and particle sizes were determined by atomic force microscopy (AFM Multimode, Nanoscope IIIa; Bruker) in contact mode.

III. RESULTS AND DISCUSSION

In order to analyze the Ge concentration of each individual sample, a $\text{Ge}_x\text{V}_{(1-x)}\text{O}_{2+y}$ (monolayer)/Si (substrate) model was used and a good fit has been obtained. The Ge content for each sample is given in Table I. The energy spectra of the backscattered ions are displayed in Fig. 1, where the yield of backscattered He ions is plotted against the channel number (backscattering energy). The Ge contribution is seen at high backscattering energies (high channel number) and is partly superposed on the V signal. At lower energies, the oxygen component is superposed on the Si substrate signal.

The simulated spectrum fits the experimental RBS data. As expected, by increasing the applied power on the Ge

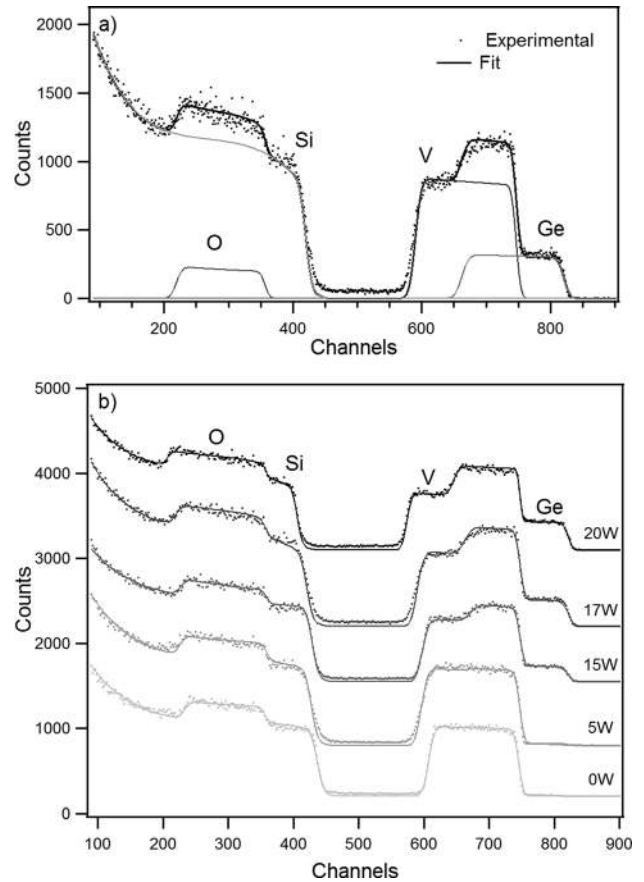


FIG. 1. (a) Experimental data (points) and simulated RBS spectra (solid line) of the $\text{Ge}_{0.059}\text{V}_{0.941}\text{O}_{2+y}$ film. The result of the simulation agrees well with the experimental RBS spectrum. (b) Comparison of VO_2 and increasingly doped $\text{Ge}_x\text{V}_{(1-x)}\text{O}_{2+y}$ films by varying the applied power on the Ge target. The width of the V and O signals is related to the film thickness, while the peak height gives indication on the concentration of backscattered ions.

target, the Ge concentration of the deposited films gradually increases.

The results of the four-point probe resistivity measurements are displayed in Fig. 2. The temperature dependent electrical resistivities were plotted for all samples, except $\text{Ge}_{0.086}\text{V}_{0.914}\text{O}_{2+y}$, for which the resistivity was too high and did not allow for a reliable reading.

The obtained curves reveal the strong influence of Ge on the switching characteristics. In order to quantitatively investigate these properties and precisely determine the phase transition temperature and hysteresis parameters, the derivatives of the resistivity variation curves, $\log \rho(T)$ vs. T , are plotted for both heating and cooling directions.

The resulting curves are fitted with Gaussian functions whose well-defined minima are taken as the phase transition temperature during heating, T_h , and cooling, T_c . Thus, the SMT is characterized by (i) the phase transition temperature, T_{SMT} , defined as the average value of the transition temperature in heating and cooling cycles,

$$T_{SMT} = 1/2 \cdot (T_h + T_c), \quad (1)$$

(ii) the hysteresis width ΔT_i , taken as the difference between T_h and T_c , and (iii) the full width at half maximum (FWHM) of the derivative curve describing the sharpness of the

TABLE I. Ge at. % as determined by the RBS measurement.

Power applied to the Ge target (W)	0	5	15	17	20
Ge content (at. %)	0.1 ± 0.1	0.5 ± 0.1	4.3 ± 0.2	5.9 ± 0.3	8.6 ± 0.4

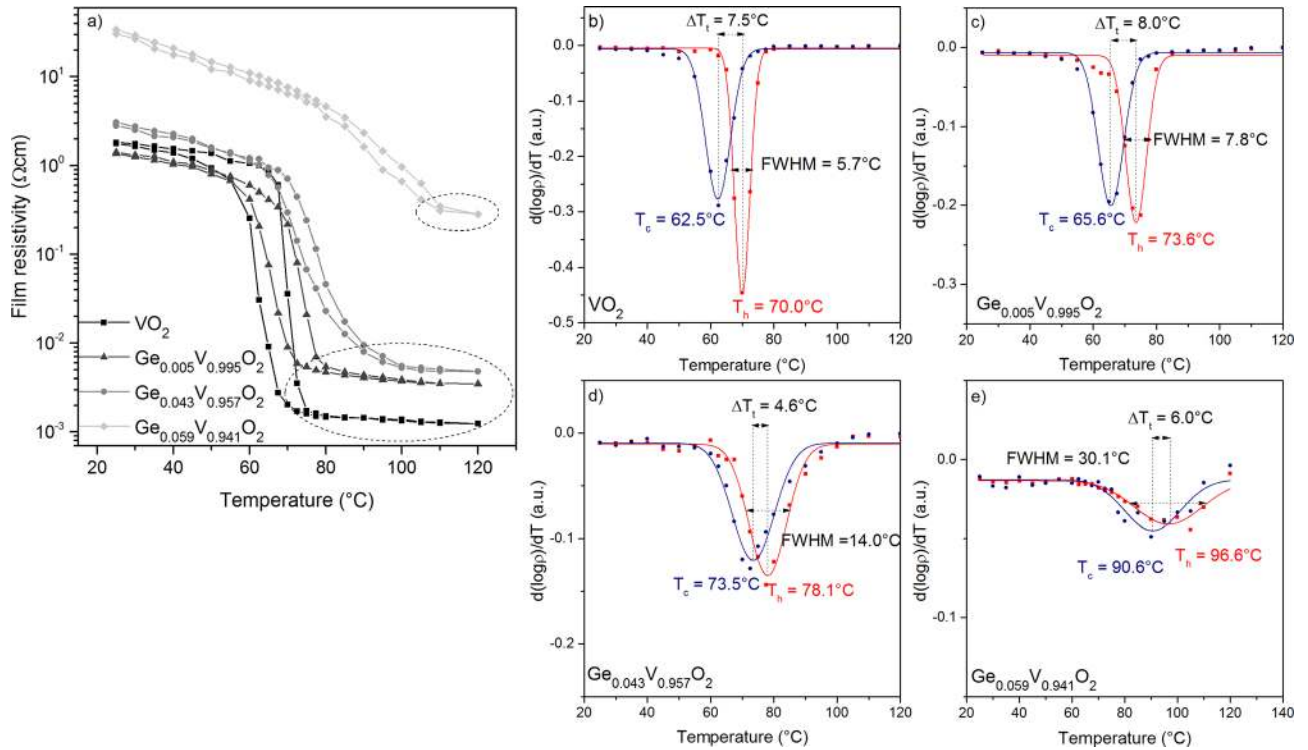


FIG. 2. (a) Temperature dependent electrical resistivities of VO_2 and $\text{Ge}_x\text{V}_{1-x}\text{O}_{2+y}$ films on Si (100) substrates. The transition temperature progressively increases with the Ge content. (b)–(e) The $d(\log \rho)/dT$ vs T curves are plotted for all samples. Measured data points (symbols) are fitted with Gaussian functions (lines) whose minima denote the transition temperatures upon heating, T_h , and cooling, T_c . The difference between T_h and T_c gives the hysteresis width, ΔT_t , while the FWHM determines the sharpness of the semiconductor-to-metal transition.

transition. The smaller value means the sharper change in the slope. The detailed parameters are summarized in Table II.

The transition temperature is gradually shifted to higher values upon doping, and it increases swiftly at higher Ge concentrations. This shift towards increased T_{SMT} might suggest a stabilization of the low temperature, monoclinic phase. A notable increase in the transition temperature occurs only at rather high Ge concentrations, e.g., ~ 6 at. %. This is in accordance with previous studies where transition temperatures were observed to change significantly only for relatively large impurity concentrations exceeding 1 at. %.^{3,23}

Film resistivities increase as well, mainly in the high temperature phase. This in turn leads to lowered amplitude modulation of the SMT. The transition magnitude is slowly lowered from ~ 3 orders, for the pure VO_2 sample, to just slightly more than 1 order for the sample with 5.9 at. % Ge. However, it is possible that this effect is due to non-stoichiometric oxygen in doped $\text{Ge}_x\text{V}_{1-x}\text{O}_{2+y}$ type films, induced by perturbations associated with the presence of a second plasma in the deposition chamber. A fine-tuning of the oxygen partial pressure might limit the decrease in the transition magnitude.

TABLE II. Detailed switching parameters determined for the differently doped vanadium dioxide films.

Ge content (at. %)	T_h (°C)	T_c (°C)	T_{SMT} (°C)	ΔT_t (°C)	FWHM (°C)
0.1	70.0	62.5	66.3	7.5	5.7
0.5	73.6	65.6	69.6	8	7.8
4.3	78.1	73.5	75.8	4.6	14.0
5.9	96.6	90.6	93.6	6	30.1

Finally, the FWHM steadily increases with Ge addition. Hence, the transition becomes less abrupt, extending over a wide range of temperatures. The hysteresis width is generally narrowed with Ge addition.

The samples are polycrystalline and exhibit typical diffraction peaks of the M1 VO_2 phase (space group $\text{P12}_1/\text{c1}$, $a = 0.5742(4)$, $b = 0.4521(3)$, $c = 0.5373(4)$ nm, $\alpha = 90$, $\beta = 122.60(5)$, and $\gamma = 90^\circ$).

Furthermore, no characteristic peaks of other vanadium oxide phases have been observed, indicating single phase VO_2 films. Exception from the above was the $\text{Ge}_{0.086}\text{V}_{0.914}\text{O}_{2+y}$ film with no diffraction peaks distinguishable.

For clarity, only the XRD patterns of the least and most doped samples are displayed, that of pure VO_2 and the samples with ~ 5.9 at. % and 8.6 at. % Ge (see Fig. 3). The absence of certain peaks in the pure sample ([002], [012]) suggests a textured film with a preferential orientation of the crystallites. For the film with 5.9 at. % Ge, the [002], [012] peaks are present as well. However, the intensity of the [1 1 -1] peak is much larger than that of the others peaks, indicating the preferential orientation in the (1 1 -1) direction.

At a 5.9 at. % Ge content, the film shows a small feature at $\sim 26.2^\circ$ (see the inset in Fig. 3). This has been attributed to the (011) peak of GeO_2 . Preliminary X-ray photoelectron spectra (XPS) of Ge doped vanadium oxide films with similar Ge concentrations show broad 3d Ge core level peaks between 31.2 and 32.1 eV binding energies. In this range, contributions from Ge^{2+} , Ge^{3+} , and Ge^{4+} peak components have been reported.³⁴ These observations suggest that Ge might be partly oxidized in the reactive environment during the deposition process.

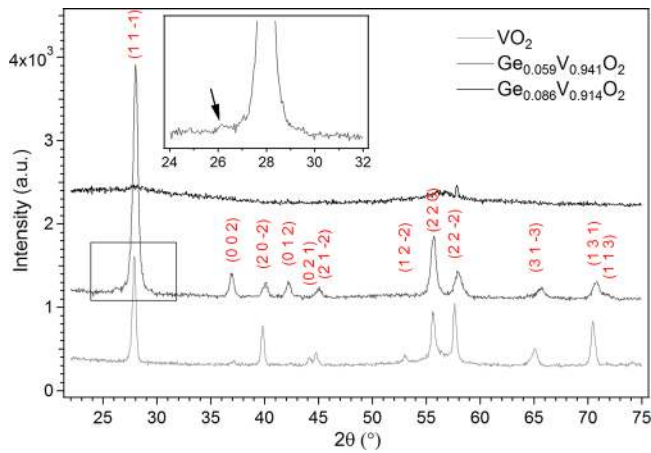


FIG. 3. XRD spectra of VO_2 , $\text{Ge}_{0.059}\text{V}_{0.941}\text{O}_{2+y}$, and $\text{Ge}_{0.086}\text{V}_{0.914}\text{O}_{2+y}$ films on the Si (100) substrate. All diffraction lines were assigned to the stoichiometric VO_2 monoclinic phase according to Ref. 33.

With doping, a shift of the diffraction peaks toward higher angles is observed. This indicates smaller distances between the crystal planes. Moreover, the broadening of the peaks, compared to the pure sample, is attributed to the

decrease in the average grain size in the polycrystalline film with doping.

The crystallite size can be determined from the peak width (FWHM) through the Scherrer equation. The peak widths are corrected with respect to the reference Si peak (the Si wafer has been measured with the same optics and under the same conditions as the deposited films). The wavelength of the Cu $K\alpha 1$ radiation is $\lambda = 1.54056 \text{ \AA}$, and the shape factor K is 0.9 for isotropic particles. In these conditions, the crystallite size is found to be $\sim 26 \text{ nm}$ in the pure VO_2 sample and $\sim 10.6 \text{ nm}$ in the film with 5.9 at. % Ge. The sample with the highest Ge content, 8.6 at. %, appears to have undergone an amorphization of the film as diffraction peaks vanished. This is consistent with the absence of the SMT during the electrical resistivity measurements discussed previously.

The evolution of the film morphology with doping has been observed from contact mode AFM images. In Fig. 4, the topographic (left) and lateral (right) AFM images of the three samples are shown.

The pure sample shows particles of variable sizes, ranging between 80 and 120 nm. At a 5.9 at. % Ge content, the particles are smaller, $\sim 40\text{--}70 \text{ nm}$ in size, and show a slightly

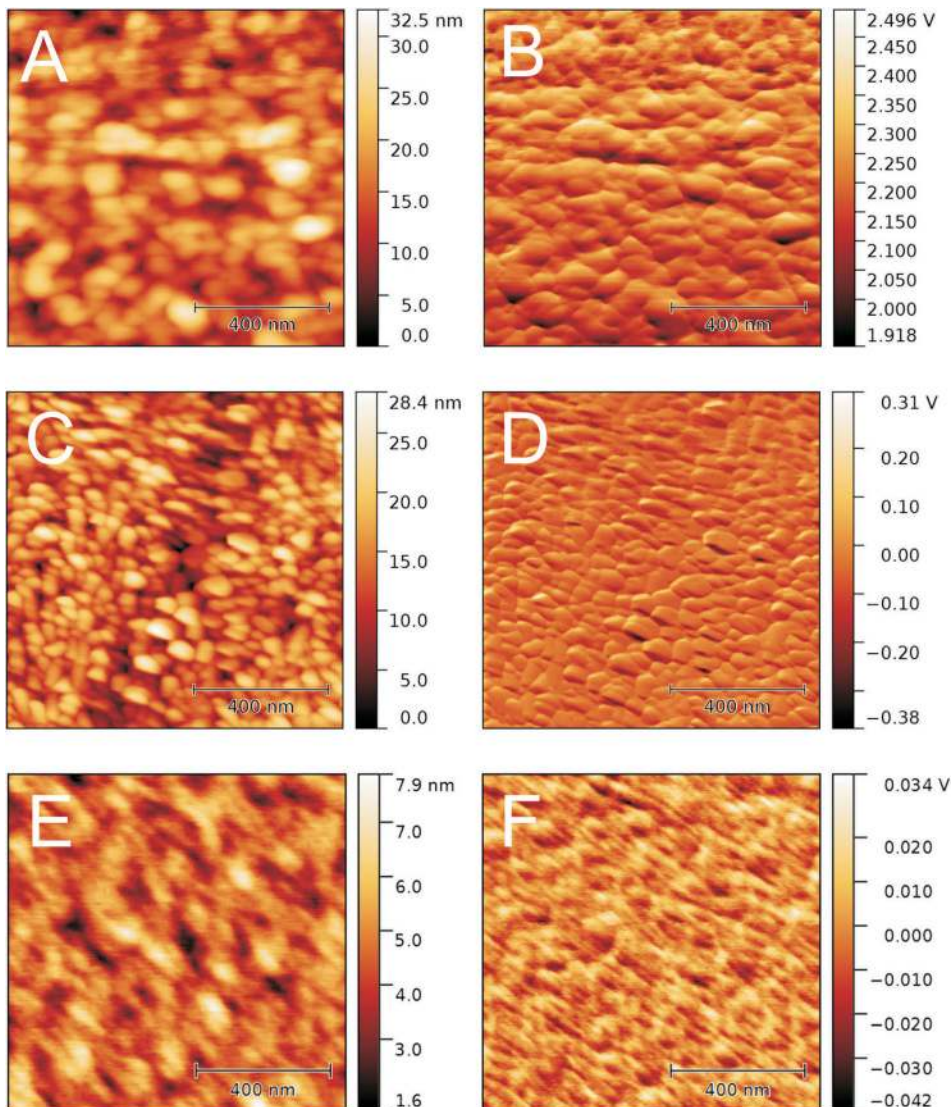


FIG. 4. Topographic (left) and lateral (right) contact mode AFM images of pure (a) and (b), $\text{Ge}_{0.059}\text{V}_{0.941}\text{O}_{2+y}$ (c) and (d), and $\text{Ge}_{0.086}\text{V}_{0.914}\text{O}_{2+y}$ (e) and (f) films. The scale bar corresponds to 400 nm.

more uniform size distribution. At an 8.6 at. % Ge concentration, the sample exhibits a smooth and uniform surface, characteristic of homogeneous, amorphous films. This general trend is in agreement with the resistivity and XRD measurements. However, the particle sizes observed using AFM considerably differ from the crystallite sizes determined from XRD peak widths. The Scherrer equation gives an approximation of the individual crystallite sizes, while the particles observed in AFM might contain several crystallites.

The decrease in the average grain size with Ge addition is expected as doping leads to disorder in the VO₂ crystal lattice. Therefore, Ge might introduce nucleation centers. The high density of nucleation centers leads to increased nucleation velocities, which, in turn, results in smaller grain sizes.

As reported in Ref. 35, the larger density of grain boundaries and associated defects could lower the resistivity of the semiconducting state, while limiting the conductivity of the metallic state through grain boundary scattering of electrons. Thus, grain refinement results in less abrupt transitions. This trend has been observed from the electrical resistivity plots.

Furthermore, even above the transition temperature, the samples exhibit a semiconducting behavior with the resistivity showing a negative temperature coefficient [indicated by dashed ellipses in Fig. 2(a)]. A small amount of other VO_x phases, which do not undergo SMT, might be present, e.g., at grain boundaries, and influence the overall resistivity of the films above T_{SMT}. The more pure the VO₂ film is, the larger is the transition amplitude. Inversely, when more non-stoichiometric VO_x is present in the film, the resistivity drop is lowered due to the enhanced semiconducting behavior above T_{SMT}.³⁶ It could be speculated then that Ge doping facilitates the formation of non-stoichiometric phases in the film. As already mentioned, an optimization of the oxygen partial pressure during deposition might counter the loss in the transition magnitude.

In addition to the decrease in the transition amplitude, the sharpness of the transition is significantly reduced upon doping—larger FWHM. As suggested in Ref. 36, a possible explanation for such smeared out transitions, spreading over temperature ranges as high as ~30 °C, may be that crystallites exhibit different SMT temperatures. The transition in the polycrystalline film occurs over the distribution of transition temperatures of the different crystallites. Such a variation in the transition temperature of individual crystallites might be strain induced. Lattice disorder, defects, and grain boundary density, in the doped films, are expected to be superior to those in pure VO₂. Ge_xV_(1-x)O_{2+y} lattices are then strained due to the stresses coming from these grain boundaries and other defects.

VO₂ bulk single crystals exhibit a very narrow hysteresis width of 0.5–1 °C.³⁷ High quality epitaxial VO₂ films show rather comparable widths of ~1.5–2 °C.^{38,39} However, polycrystalline VO₂ films might have considerably broader hysteresis loops, ranging from a few degree widths to more than 30 °C in some cases.^{36,40} The mechanism of hysteresis in both VO₂ single crystals and thin films is not fully understood. Nonetheless, in polycrystalline films, numerous factors have been reported to affect it such as the grain size,⁴¹

crystallinity,⁴² nucleation defects,⁴³ orientation of grain boundaries,⁴⁴ and grain shape.⁴⁰

In general, the hysteresis widths of our doped polycrystalline VO₂ films are smaller than that of the pure film.

In Ref. 41, a nucleation theory is proposed where the phase transition is nucleated on defects. According to this study, an increased number of nucleation seeds can potentially trigger the phase transition and lead to narrower hysteresis loops.

Ge might enhance the heterogeneous nucleation of VO₂ particles similar to Ti in VO₂.⁴³ The larger density of grain boundaries and lattice disorder could be accountable for a higher effective defect concentration in doped samples. Relatively high amounts of dopants could significantly increase the density of defect-induced nucleation sites. As a consequence, the free energy decrease for SMT is lowered and a smaller ΔT—narrower hysteresis—can trigger the transition.

Following this reasoning, other dopants might also increase the defect-nucleation site density and narrow the hysteresis, which was indeed observed experimentally.²²

The role of lattice distortion and charge doping effects on the phase transition in doped vanadium dioxide systems is still unclear. In Ref. 45 and references therein, an overview of the proposed mechanisms for the widely studied W⁶⁺ doping is presented. Several studies attribute the reduction in T_{SMT} to the increase in electron density; some claim that the effect of W⁶⁺ on neighboring cells is only structural, while others have shown that both electronic contribution and local structure perturbations are responsible for the reduced T_{SMT}. The authors of the cited study⁴⁵ agree with the latter and conclude their comparative analysis on Ti and W doped VO₂, suggesting that charge doping is more effective in regulating the transition temperature in VO₂, although the local structure perturbations induced by dopants have an inevitable influence on it. MacChesney and Guggenheim²³ also point out that, regardless of the origin of the transition, changes in the band structure are sensitive to changes in the lattice and speculate that the changes induced by dopants are the result of the interplay of the size and charge. Small cations, e.g., Al³⁺, Ga³⁺, and Ge⁴⁺, with empty d orbitals are more stable in lower anion coordination and seem to stabilize the low temperature phase. Additionally, when charge compensation is accomplished through the creation of V⁵⁺ ions—smaller than V⁴⁺, with empty d orbitals and unstable in an oxygen octahedron—a lower anion coordination is favored again.³

Nonetheless, the significant change in transition temperature reached through Ge doping—as in the case of W doping—is presumably the result of both lattice distortion and electronic effects. However, the main contributor and the way it acts on the VO₂ lattice are yet to be determined.

IV. CONCLUSIONS

Through a controlled sputtering process, pure VO₂ and Ge_xV_(1-x)O_{2+y} films have been deposited. A direct correlation between the SMT characteristics, most notably the transition temperature and doping concentration, has been established. A T_{SMT} value of ~96 °C has been reached with

5.9 at. % Ge. To the best of our knowledge, this is the highest transition temperature reported for doped VO₂ based thin films.

These findings constitute further motivation in studying doped vanadium dioxide films, which could help to advance our current understanding of the underlying fundamental principles of the semiconductor-to-metal transition in VO₂.

ACKNOWLEDGMENTS

This work was financially supported by the Swiss Federal Office of Energy (Grant No. 810002805). This work has also received partial funding from the European Union's Horizon 2020 research and innovation programme, under the FETOPEN Phase Change Switch Grant 737109. The authors are grateful to Dr. Rosendo Sanjines for the inspiring discussions.

- ¹F. J. Morin, *Phys. Rev. Lett.* **3**, 34–36 (1959).
- ²C. N. Berglund and H. J. Guggenheim, *Phys. Rev.* **185**, 1022–1033 (1969).
- ³J. B. Goodenough, *J. Solid State Chem.* **3**, 490–500 (1971).
- ⁴A. Cavalleri, T. Dekorsy, H. H. W. Chong, J. C. Kieffer, and R. W. Schoenlein, *Phys. Rev. B - Condens. Matter Mater. Phys.* **70**, 161102(R) (2004).
- ⁵A. Cavalleri, C. Tóth, C. W. Siders, J. A. Squier, F. Ráksi, P. Forget, and J. C. Kieffer, *Phys. Rev. Lett.* **87**, 237401 (2001).
- ⁶A. S. Barker, H. W. Verleur, and H. J. Guggenheim, *Phys. Rev. Lett.* **17**, 1286–1289 (1966).
- ⁷A. Paone, R. Sanjines, P. Jeanneret, and A. Schüler, *Sol. Energy* **118**, 107–116 (2015).
- ⁸J.-C. Orlianges, J. Leroy, A. Crunteanu, R. Mayet, P. Carles, and C. Champeaux, *Appl. Phys. Lett.* **101**, 133102 (2012).
- ⁹S. Lee, K. Hippalgaonkar, F. Yang, J. Hong, C. Ko, J. Suh, K. Liu, K. Wang, J. J. Urban, X. Zhang, C. Dames, S. A. Hartnoll, O. Delaire, and J. Wu, *Science* **355**, 371–374 (2017).
- ¹⁰H. Wang, X. Yi, S. Chen, and X. Fu, *Sens. Actuators, A* **122**, 108–112 (2005).
- ¹¹W. A. Vitale, E. A. Casu, A. Biswas, T. Rosca, C. Alper, A. Krammer, G. V. Luong, Q.-T. Zhao, S. Mantl, A. Schüler, and A. M. Ionescu, *Sci. Rep.* **7**, 355 (2017).
- ¹²W. A. Vitale, L. Petit, C. F. Moldovan, M. Fernández-Bolanos, A. Paone, A. Schüler, and A. M. Ionescu, *Sens. Actuators, A* **241**, 245–253 (2016).
- ¹³N. Émond, A. Hendaoui, and M. Chaker, *Appl. Phys. Lett.* **107**, 143507 (2015).
- ¹⁴C. G. Granqvist, *Thin Solid Films* **193–194**, 730–741 (1990).
- ¹⁵L. Zhao, L. Miao, C. Liu, C. Li, T. Asaka, Y. Kang, Y. Iwamoto, S. Tanemura, H. Gu, and H. Su, *Sci. Rep.* **4**, 7000 (2014).
- ¹⁶A. Paone, M. Geiger, R. Sanjines, and A. Schüler, *Sol. Energy* **110**, 151–159 (2014).
- ¹⁷M. Benkahoul, M. Chaker, J. Margot, E. Haddad, R. Kruzelecky, B. Wong, W. Jamroz, and P. Poinas, *Sol. Energy Mater. Sol. Cells* **95**, 3504–3508 (2011).
- ¹⁸R. M. Wentzcovitch, W. W. Schulz, and P. B. Allen, *Phys. Rev. Lett.* **72**, 3389–3392 (1994).
- ¹⁹T. M. Rice, H. Launois, and J. P. Pouget, *Phys. Rev. Lett.* **73**, 3042–3042 (1994).
- ²⁰A. Zylbersztejn and N. F. Mott, *Phys. Rev. B* **11**, 4383–4395 (1975).
- ²¹S. Biermann, A. Poteryaev, A. I. Lichtenstein, and A. Georges, *Phys. Rev. Lett.* **94**, 026404 (2005).
- ²²A. Paone, R. Sanjines, P. Jeanneret, H. J. Whitlow, E. Guibert, G. Guibert, F. Bussy, J.-L. Scartezzini, and A. Schüler, *J. Alloys Compd.* **621**, 206–211 (2015).
- ²³J. B. MacChesney and H. J. Guggenheim, *J. Phys. Chem. Solids* **30**, 225–234 (1969).
- ²⁴H. Futaki and M. Aoki, *Jpn. J. Appl. Phys., Part 1* **8**, 1008–1013 (1969).
- ²⁵I. Kitahiro and A. Watanabe, *Jpn. J. Appl. Phys., Part 1* **6**, 1023–1024 (1967).
- ²⁶B. Chen, D. Yang, P. A. Charpentier, and M. Zeman, *Sol. Energy Mater. Sol. Cells* **93**, 1550–1554 (2009).
- ²⁷A. Gentle and G. B. Smith, *J. Phys. D: Appl. Phys.* **41**, 015402 (2008).
- ²⁸T. E. Phillips, R. A. Murphy, and T. O. Poehler, *Mater. Res. Bull.* **22**, 1113–1123 (1987).
- ²⁹B. L. Brown, M. Lee, P. G. Clem, C. D. Nordquist, T. S. Jordan, S. L. Wolfley, D. Leonhardt, C. Edney, and J. A. Custer, *J. Appl. Phys.* **113**, 173704 (2013).
- ³⁰H. Futaki, K. Kobayashi, M. Aoki, T. Shimoda, E. Yamada, and K. Narita, U.S. patent 3,402,131 (17 September 1968).
- ³¹A. Krammer, A. Gremaud, O. Bouvard, R. Sanjines, and A. Schüler, *Surf. Interface Anal.* **48**, 440–444 (2016).
- ³²N. P. Barradas, C. Jeynes, and R. P. Webb, *Appl. Phys. Lett.* **71**, 291 (1997).
- ³³J. C. Rakotoniaina, R. Mokrani-Tamellin, J. R. Gavarrí, G. Vacquier, A. Casalot, and G. Calvarin, *J. Solid State Chem.* **103**, 81–94 (1993).
- ³⁴A. Molle, N. K. Bhuiyan, G. Tallarida, and M. Fanciulli, *Appl. Phys. Lett.* **89**, 083504 (2006).
- ³⁵D. Brassard, S. Fourmaux, M. Jean-Jacques, J. C. Kieffer, and M. A. El Khakan, *Appl. Phys. Lett.* **87**, 051910 (2005).
- ³⁶D. Ruzmetov, K. T. Zawilski, V. Narayanamurti, and S. Ramanathan, *J. Appl. Phys.* **102**, 113715 (2007).
- ³⁷L. A. Ladd and W. Paul, *Solid State Commun.* **7**, 425–428 (1969).
- ³⁸P. J. Hood and J. F. Denatale, *J. Appl. Phys.* **70**, 376–381 (1991).
- ³⁹P. Jin, K. Yoshimura, and S. Tanemura, *J. Vac. Sci. Technol., A* **15**, 1113 (1997).
- ⁴⁰H. Zhang, Z. Wu, D. Yan, X. Xu, and Y. Jiang, *Thin Solid Films* **552**, 218–224 (2014).
- ⁴¹R. Lopez, T. E. Haynes, L. A. Boatner, L. C. Feldman, and R. F. Haglund, *Phys. Rev. B* **65**, 224113 (2002).
- ⁴²J. Y. Suh, R. Lopez, L. C. Feldman, and R. F. Haglund, *J. Appl. Phys.* **96**, 1209–1213 (2004).
- ⁴³J. Du, Y. Gao, H. Luo, L. Kang, Z. Zhang, Z. Chen, and C. Cao, *Sol. Energy Mater. Sol. Cells* **95**, 469–475 (2011).
- ⁴⁴J. Narayan and V. M. Bhosle, *J. Appl. Phys.* **100**, 103524 (2006).
- ⁴⁵Y. Wu, L. Fan, Q. Liu, S. Chen, W. Huang, F. Chen, G. Liao, C. Zou, and Z. Wu, *Sci. Rep.* **5**, 9328 (2015).